Melanopsin-mediated post-illumination pupil response in the peripheral retina

Daniel S. Joyce

Institute of Health and Biomedical Innovation, Queensland University of Technology (QUT), Brisbane, Australia
School of Optometry and Vision Science, Queensland University of Technology (QUT), Brisbane, Australia

Beatrix Feigl

Institute of Health and Biomedical Innovation, Queensland University of Technology (QUT), Brisbane, Australia
School of Biomedical Sciences, Queensland University of Technology (QUT), Brisbane, Australia
Queensland Eye Institute, Brisbane, Australia

Andrew J. Zele

Institute of Health and Biomedical Innovation, Queensland University of Technology (QUT), Brisbane, Australia
School of Optometry and Vision Science, Queensland University of Technology (QUT), Brisbane, Australia

Intrinsically photosensitive retinal ganglion cells (ipRGCs) regulate pupil size by integrating extrinsic rod and cone signals with intrinsic melanopsin-mediated phototransduction. Light adapted pupil diameter is determined by the corneal flux density (CFD), and for central visual field stimulation the melanopsin-mediated post-illumination pupil response (PIPR) follows this same CFD relationship. Rods, cones, and ipRGCs vary in size, density, and distribution across the retina, but how these differences affect the amplitude and timing of the extrinsic and intrinsic pupil light reflex in the central and peripheral retina is unknown. We determined the relationship between stimulus area and photon flux with stimuli constant for CFD, irradiance, or area at central (0°) and peripheral (20°) eccentricities with high and low melanopsin excitation. We show that the pupil constriction amplitude was similar at both eccentricities and the time to minimum diameter increased as melanopsin excitation increased. In contrast, the peripheral PIPR follows a CFD relationship but with lower amplitude compared with that at the fovea. This indicates differences in the spatial and temporal characteristics of extrinsic and intrinsic ipRGC inputs to the pupil control pathway for the central and peripheral retina. The eccentricity-dependent change in PIPR amplitude may be analogous to the hill of vision observed in visual perimetry; such knowledge is an important precursor to the development of pupil perimetry paradigms to measure the PIPR in select regions of the visual field.

Introduction

For central visual field stimulation the light adapted steady-state pupil diameter is determined by the product of stimulus area and luminance, the corneal flux density (CFD) (Atchison et al., 2011; Crawford, 1936; Park & McAnany, 2015; Stanley & Davies, 1995; Vervoort, 1899; Watson & Yellott, 2012), whereby doubling stimulus area and halving luminance has the same (null) effect upon pupil diameter as the converse relationship.

Citation: Joyce, D. S., Feigl, B., & Zele, A. J. (2016). Melanopsin-mediated post-illumination pupil response in the peripheral retina. *Journal of Vision*, *16*(8):5, 1–15, doi:10.1167/16.8.5.

doi: 10.1167/16.8.5 Received November 25, 2015; published June 6, 2016 ISSN 1534-7362

With on-axis foveated stimuli, the intrinsic melanopsin-mediated post-illumination pupil response (PIPR) follows this CFD relationship for dark adapted stimuli; however, the light adapted extrinsic cone inputs to intrinsically photosensitive retinal ganglion cells (ipRGCs) that mediate the constriction amplitude do not (Park & McAnany, 2015), indicating a complex interaction between outer and inner retinal processing to control the pupil light reflex in response to central stimulation. With peripheral stimulation, the steady-state pupil diameter is similar (Spring & Stiles, 1948) or reduced (Jay, 1962) to that of the central retina and the absolute (millimeter) pupil constriction amplitude is reduced compared with the central retina (Hong, Narkiewicz, & Kardon, 2001; Schweitzer, 1956; Skorkovská, Wilhelm, Lüdtke, Wilhelm, & Kurtenbach, 2014). The effects of stimulus area and luminance on the PIPR in the peripheral retina have not been investigated.

The pupil response to light is controlled by extrinsic rod and cone and intrinsic melanopsin signals mediated by ipRGC inputs to the pretectum (for review, see Feigl & Zele, 2014; McDougal & Gamlin, 2015). Given that the outer retinal rod and cone photoreceptors have different topographical distributions and temporal and spatial summation properties to inner retinal ipRGCs, the extrinsic inputs to the pupil constriction may show different response characteristics in the peripheral and central retina compared with the intrinsic PIPR. In human and macaque retinae, ipRGCs are absent in the fovea, peak parafoveally (~7.7°) and decrease in number with increasing eccentricity, reaching a plateau at ~26.7° whereas their dendritic field size linearly increases threefold between ~0.25° and ~33.3° (Dacey et al., 2005; Drasdo & Fowler, 1974; Liao et al., 2016). It is not known how this tradeoff between receptive field size and density manifests in the pupil light reflex. If ipRGC density is the primary determinant of intrinsic photon capture by ipRGCs and thus PIPR amplitude, we hypothesize that PIPR amplitude will decrease with increasing eccentricity. Alternatively, if ipRGC dendritic field diameter is the primary determinant of the PIPR, then PIPR amplitude will increase in the peripheral retina. However, ipRGCs connect to one another via gap junctions to form a lateral plexus, effectively a larger photoreceptive net across the retina (Hankins, Peirson, & Foster, 2008; Provencio, Rollag, & Castrucci, 2002; Sekaran, Foster, Lucas, & Hankins, 2003) and this may negate any effect of eccentricity on the melanopic pupil response. Here, we explore whether the ipRGC-mediated pupil constriction amplitude (extrinsic and intrinsic pathway) and post-illumination pupil response (intrinsic pathway) can be described by the same CFD relationship in the peripheral retina as for the central retina.

Methods

Participants

Eight observers were recruited, four in each of the 100 ms (four females, mean age 21.5 years, *SD* 1.3) and 1-s stimulus conditions (one female, mean age 31.8 years, *SD* 4.9). Author DSJ was a participant in the 1-s condition. Participants underwent an ophthalmological examination prior to the experimental session to ensure normal vision including best-corrected visual acuity, slit-lamp examination, intraocular pressure with tonometry (Icare, Vantaa, Finland), ophthalmoscopy, color vision (desaturated Lanthony D15, Richmond Products, Albuquerque, NM), and OCT (Cirrus HD-OCT, Carl Zeiss Meditec, Dublin, CA). All participants had best-corrected visual acuity of 6/6 or better and normal eye health.

The project was approved by the University's Human Research Ethics committee (ethics number 1400000842) and experiments were conducted in accordance with the Code of Ethics of the World Medical Association (Declaration of Helsinki). Participants provided informed consent before the experiments began.

Apparatus

The Maxwellian-view pupillometer optics are reported elsewhere (Joyce, Feigl, Cao, & Zele, 2015). The irradiances of the short wavelength (blue appearing λ_{max} 464 nm, FWHM 20 nm) and long wavelength (red appearing λ_{max} 658 nm, FWHM 22 nm) 5 mm stimulus LEDs were precisely controlled electronically (software digital-to-analog converter values) and attenuated using calibrated neutral density filters (Ealing, Natick, MA). Stimulus diameter was controlled via a 50-mm aperture (Thorlabs, Newton, NJ) positioned in the pupillometer at the common focal position between two Fresnel lenses (100 mm diameter, 127 mm, and 70 mm focal lengths; Edmund Optics, Singapore). Stimuli were presented in Maxwellian-view to the participant's left eye and the consensual response of the right eye was recorded in monochrome (PixeLINK PL-B741 FireWire, 640 × 480 pixels, Ottawa, ON, Canada) at 60 Hz under infrared illumination (λ_{max} 851 nm). Alignment in the optical system was maintained with a chin rest, temple bars, and head restraint. Pupil analyses were performed offline using a program custom coded in Xcode (version 3.3.3.5).

Experimental design

In humans, the extrinsic and intrinsic ipRGC pathways control the amplitude and timing of the pupil constriction

	α-Opic lux									
Photoreceptor excitation	464 nm	658 nm	464 nm	658 nm	464 nm	658 nm	464 nm	658 nm	464 nm	658 nm
Log photons.cm^{-2}.s^{-1}	13.70	13.70	13.95	13.95	14.30	14.30	14.90	14.90	15.50	15.50
Log cd.m^{-2}	1.22	1.35	1.45	1.60	1.79	1.98	2.34	2.53	2.94	3.11
S-cone	169.80	0.00	301.00	0.00	673.39	0.00	2680.07	0.00	10,668.17	0.00
Melanopsin	136.81	0.01	242.53	0.02	542.57	0.05	2159.42	0.19	8595.69	0.75
Rod	95.41	0.08	169.14	0.15	378.39	0.33	1505.99	1.33	5994.68	5.30
M-cone	46.14	1.91	81.79	3.41	182.97	7.61	728.20	30.25	2898.65	120.42
L-cone	23.66	12.37	41.94	22.09	93.83	49.25	373.45	195.68	1486.53	778.96

Table 1. Photoreceptor excitations (specified in α-opic lux) as a function of corneal irradiance and luminance.

(Kardon et al., 2009). The dark adapted PIPR in the central retina is controlled by the intrinsic melanopsin ipRGC pathway, with its spectral sensitivity in response to high irradiance stimuli matching that of a single vitamin A photopigment nomogram with a peak at ~482 nm (Adhikari, Zele, & Feigl, 2015; Gamlin et al., 2007; Markwell, Feigl, & Zele, 2010). The α-opic photoreceptor excitations (Lucas et al., 2014) of the stimuli show that the melanopic excitation of the highest corneal irradiance (15.5 log photons.cm^{-2}.s^{-1}) short wavelength light was ~11,460× greater than its long wavelength counterpart (Table 1). Therefore, the short wavelength high irradiance stimulus light has the highest melanopsin excitation, and so during light exposure the pupil constriction is dependent on intrinsic and extrinsic signalling, and after light offset the PIPR amplitude is entirely mediated by intrinsic signalling. In contrast, the long wavelength stimulus lights (of all irradiances) have low melanopsin excitation and thus the PLR in response to long wavelength light is predominantly driven by extrinsic photoreceptor inputs to the ipRGC pathway. Note that a high or low photoreceptor excitation does not imply the presence (or absence) of its functional contribution to the pupil. Photoreceptor contributions to the pupil control pathway have been defined under light adapted conditions using silent substitution with multi-primary photostimulation methods (Barrionuevo et al., 2014; Cao, Nicandro, & Barrionuevo, 2015; Spitschan, Jain, Brainard, & Aguirre, 2014; Tsujimura, Ukai, Ohama, Nuruki, & Yunokuchi, 2010; Viénot, Bailacq, & Rohellec, 2010), but the relationships between α-opic lux, extrinsic and intrinsic ipRGC signalling and the dark adapted pupil response are yet to be characterized (Joyce et al., 2015; Lucas et al., 2014). In addition, α-opic lux does not account for any potential effects of changes in prereceptoral filtering or spectral sensitivity that might occur in the peripheral retina and with different field sizes (Kokoschka & Adrian, 1985; Stabell & Stabell, 1980; van Esch, Koldenhof, van Doorn, & Koenderink, 1984).

To investigate how the changes in ipRGC density and dendritic field diameter with eccentricity affect the timing and amplitude of the PLR, stimuli were presented at central (0°) and peripheral (20°) eccentricities. For the central condition observers fixated on-axis in the center of the Fresnel lens. For the peripheral condition observers fixated upon a small (<0.5°) dim red target projected onto the surface of the Fresnel lens for temporal retina stimulation (nasal hemifield) of the left eye. Because spatial and temporal summation are interdependent (Barlow, 1958) and vary with eccentricity (Wilson, 1970), we used stimuli that were longer than the threshold pupil critical duration for central field presentations (Alpern, McCready, & Barr, 1963; Webster, 1969). To determine if the area of spatial summation changed with duration, 100-ms and 1-s stimuli were used.

Three experimental conditions were designed to evaluate interactions between stimulus irradiance and area upon the pupil response: (1) The constant corneal flux density (CFD) condition tested the hypothesis that the irradiance and stimulus area are reciprocal in the peripheral retina for the pupil constriction and PIPR. The CFD relationship was maintained such that when stimulus area doubled, the irradiance was halved; irradiance (diameter) combinations were 15.50 (5°), 14.90 (10°), 14.30 (20°), 13.95 (30°), and 13.70 (40°) log photons.cm^{-2}.s^{-1}. (2) The constant irradiance condition ascertained whether the peripheral pupil response is determined by field size; the irradiance was fixed at 14.9 log photons.cm^{-2}.s^{-1} and field size varied between 5° and 40° diameter. (3) The constant diameter condition assessed if the peripheral pupil response is determined by irradiance; the stimulus diameter was 40° and irradiance varied between 13.70 and 15.50 log photons.cm^{-2}.s^{-1}.

Wavelength dependent attenuation by the optical media of the eye changes with age (Wooten, Hammond, Land, & Snodderly, 1999; Xu, Pokorny, & Smith, 1997), and so we used the van de Kraats and van Norren (2007) model of the optical density of the media (lens, cornea, aqueous, and vitreous humors) for stimuli greater than 3° diameter to estimate the retinal irradiances of the short and long wavelength stimuli. The mean optical attenuation for short wavelength stimuli (465 nm) was 0.28 for the participants who completed the 100-ms condition and 0.31 log units for participants who completed the 1-s condition (3.5% difference between participant groups), and for long

wavelength stimuli (658 nm) the attenuation was 0.15 log units for both groups.

Procedure

One drop of tropicamide 1% (Minims, Chauvin Pharmaceuticals Ltd., Romford, UK) was applied to the participant's left eye. When the pupil was fully dilated (mean 7.46 mm, *SD* 0.89), the participant was aligned in the pupillometer and dark adapted for 8 min to minimize the influence of prior light exposure on the pupil. Each pupil recording consisted of a 13-s baseline, 100-ms or 1-s stimulus, and a 40-s post-stimulus period. Two repeats were obtained in a single session and each participant provided a total of four repeats for each of the three conditions (CFD, constant irradiance, and constant diameter) at two eccentricities (0° and 20°) for one duration only (100 ms or 1 s; total individual participant testing time ~18 hr). To allow the PIPR to return to baseline, stimuli were separated by at least 2 min (Adhikari et al., 2015) in the darkened laboratory during which time the participants could remove their head from the pupillometer but remained seated. Stimuli were presented from low to high irradiance to minimize adaptation effects and alternated between long and short wavelengths to control for the reported bistability (Mure et al., 2009; Mure, Rieux, Hattar, & Cooper, 2007) or tristability (Emanuel & Do, 2015) of the melanopsin chromophore. Each participant was tested either in the morning or afternoon to avoid attenuation of the PIPR amplitude, which occurs in the evening nearer to the time of melatonin onset (Zele, Feigl, Smith, & Markwell, 2011).

Data analysis

Artifacts from blinks not automatically rejected by the pupil measurement algorithm were manually removed upon visual inspection, and the data were smoothed using a second order polynomial averaging 20 neighbors (333-ms window). Analyses with more than 20% data loss were rejected and remeasured. The pupil appears elliptical to the plane of the camera when recorded off-axis during the peripheral condition and this can underestimate the true pupil size (for review see Mathur, Gehrmann, & Atchison, 2013). Therefore, to facilitate comparison between central and peripheral eccentricities, and to account for individual differences in resting pupil diameter (Pokorny & Smith, 1997), the data were normalized to the average diameter during the 5-s preceding stimulus onset.

Analysis variables included time and amplitude of the minimum pupil diameter (minimum constriction amplitude), 6-s PIPR (Park et al., 2011) and the mean PIPR amplitude from 10-s to 30-s post-stimulus offset (plateau PIPR) as these two PIPR metrics have been shown to have the lowest coefficients of variation (Adhikari et al., 2015). The plateau and 6-s PIPR showed the same trends and so we report only the 6-s PIPR (referred to as PIPR hereon). To determine the effect of the three experimental conditions (CFD, constant irradiance, and constant field diameter) on the pupil response, the averaged data from the four observers in each condition for each eccentricity and duration were modelled with linear regression using a 5% significance level (GraphPad Prism 6.07, San Diego, CA). F-tests for lack of fit confirmed the adequacy of the linear regression models ($p > 0.05$). If the slope for an experimental condition did not differ from zero, then that parameter (e.g., CFD, constant irradiance, constant diameter) determined the amplitude of pupil response. Planned comparisons of slope equivalences for eccentricity and duration assessed whether a common process mediated the pupil response for that experimental condition. Repeated-measures analysis of variance (ANOVAs; $\alpha = 0.05$, Greenhouse–Geisser corrected) assessed the vertical offsets between regression lines to determine the effect of stimulus eccentricity and duration upon the amplitude of the pupil response within each experimental condition. An a priori sample size calculation was not performed due to the unknown properties of the peripheral PIPR, but the significant difference in mean short wavelength PIPR amplitude with eccentricity demonstrates that the sample size was sufficient (post-hoc effect size Cohen's $d_z = 1.59$, power = 0.58).

Results

Mean pupil tracings for the first 15 s after stimulus onset for the short wavelength condition (Figure 1) show that the average minimum constriction amplitude is similar in the central (57.2% baseline) and peripheral (59.8% baseline) visual fields within each duration across the three experimental conditions (Figure 2D, E, F). The effect of eccentricity was significant only for the 1-s constant irradiance condition (mean central reduction 5.1%, Figure 2E squares). Vertical separation of the regression lines confirm the larger constriction in response to the 1-s stimuli (mean difference 13.6%; Figure 2D, E, F). The time to minimum pupil diameter for the short wavelength stimuli (Figure 2A, B, C) is on average 204.0 ms faster in the periphery. In the CFD condition the timing is slower in the central visual field as field size increases for 100-ms stimuli (slope +3.3 ms/°) but not for the 1-s stimuli (Figure 2A). The time to minimum pupil diameter slows with increasing field size (on average 319 ms slower at 40° compared with 0°, Figure 2B) and higher irradiances (on average 606.0 ms slower at 15.5 log photons.cm^{-2}.s^{-1} compared with

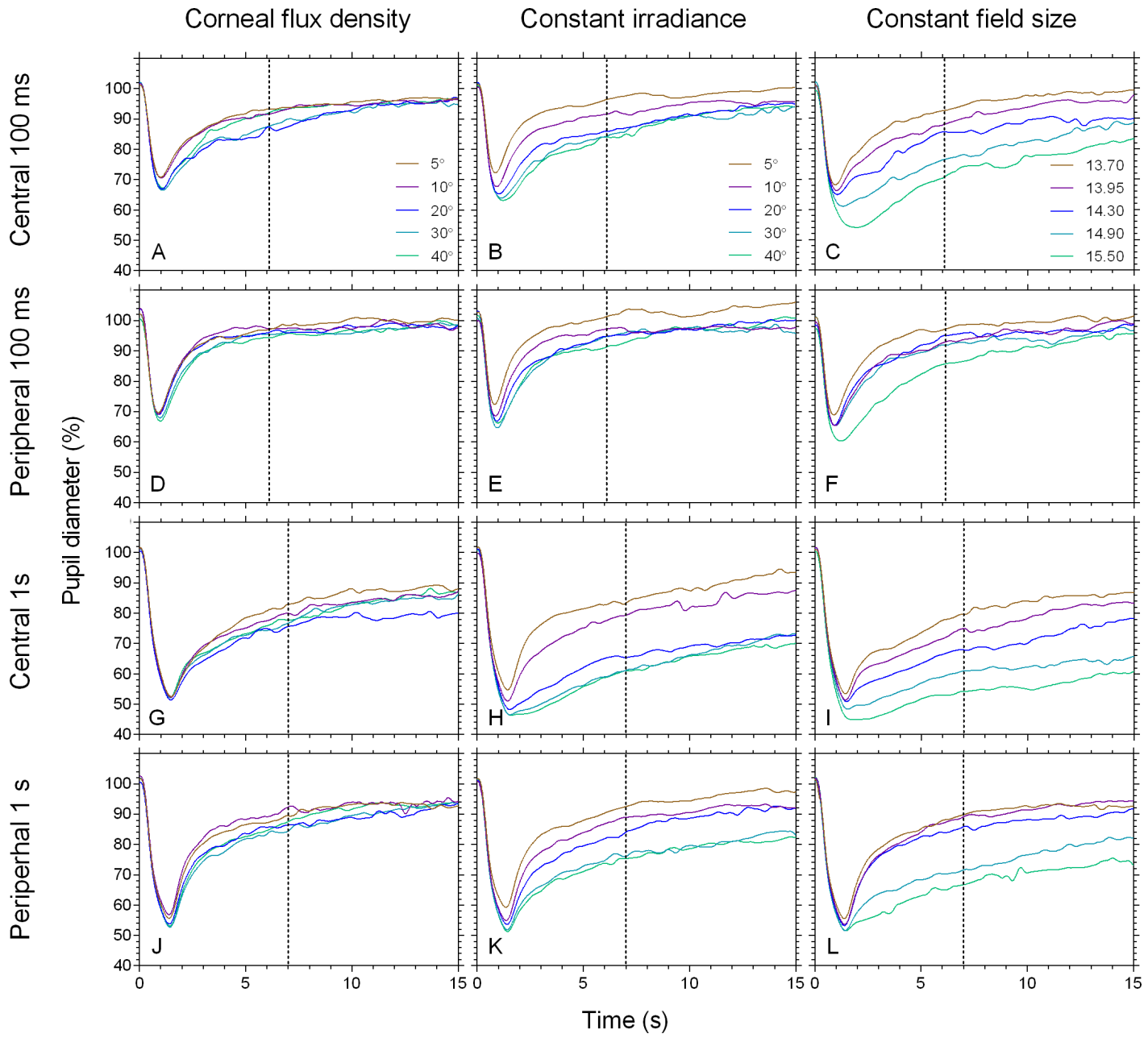

Figure 1. Mean short wavelength pupil tracings for the CFD, constant irradiance, and constant field size conditions ($n = 4$). Normalized (percentage baseline) short wavelength pupil responses are shown as a function of stimulus eccentricity (central 0° and peripheral 20°) and duration (100 ms and 1 s) for 15-s post-stimulus onset (legends are in panels A, B, and C, respectively; panel C legend is in log photons.cm^{-2}.s^{-1}). Dashed vertical lines represent the time the PIPR was quantified.

13.7 log photons.cm^{-2}.s^{-1}, Figure 2C). The slopes of the regression lines were steeper for the central data (constant irradiance slope +15.4 ms/°, constant field slope +482.6 ms/log photon.cm^{-2}.s^{-1}) than for the peripheral data (constant irradiance slope +2.7 ms/°, constant field slope +169.8 ms/log photon.cm^{-2}.s^{-1}).

The short wavelength post-illumination pupil response exhibits a different pattern to the minimum constriction amplitude; the PIPR amplitude is systematically less sustained in the peripheral retina compared with central retina for both stimulus durations (Figure 3) across all conditions (Figure 2G, H, I). Vertical separation of the regression lines confirm the larger PIPR amplitudes in response to the 1-s stimuli (mean difference 9.6%; Figure 2G, H, I). The slopes of the PIPR regression lines differ for the three experimental conditions, reflecting the contributions of stimulus irradiance and field size to the PIPR amplitude. With constant CFD the mean tracing amplitudes are similar in Figure 1A, D, G, J,

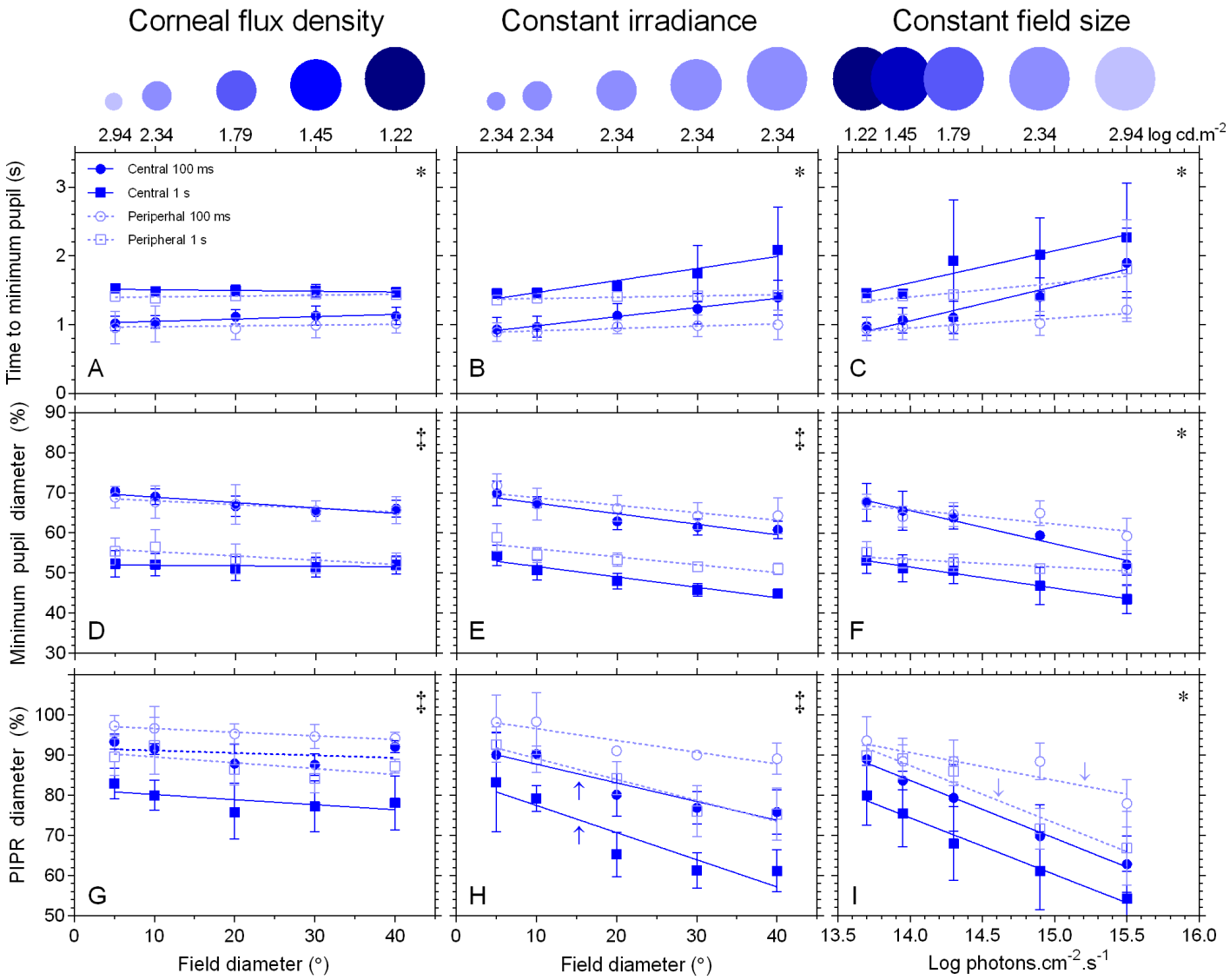

Figure 2. Time to minimum amplitude, minimum amplitude, and PIPR metrics for short wavelength stimuli (±*SD*, $n = 4$). Linear regression analysis is shown for the CFD, constant irradiance, and constant field diameter conditions as a function of stimulus eccentricity (central 0° and peripheral 20°) and duration (100 ms and 1 s). * denotes the slopes of all four regression lines are not statistically the same. ‡ denotes the absolute vertical separation of the slopes are statistically different (only determined if slopes are equivalent). A schematic representation of the stimulus diameter and irradiance are shown above the top panels; the log cd.m^{-2} values of the stimuli are indicated on the upper abscissa for the three experimental conditions. Arrows are referred to in the Discussion.

with the slopes not showing any significant difference from zero (Figure 2G), which indicates reciprocity between stimulus area and corneal irradiance in the central and peripheral retina for both durations. With constant irradiance the PIPR increases with increasing field diameter and shares a common slope (–0.5%/°) for all stimulus duration and eccentricity combinations (Figure 2H). With constant field diameter the PIPR amplitude increases with increasing irradiance, whereas the slope of the 100-ms peripheral data is shallower (–6.9%/log photon.cm^{-2}.s^{-1}) than for the other three eccentricity and duration combinations (–14.3%/log photon.cm^{-2}.s^{-1}, Figure 2I). Figures 4A and B show the PIPR replotted as a function of CFD for the constant irradiance and constant field diameter conditions respectively, and thus show similar trends to Figures 2H and I.

For the long wavelength data with low melanopsin excitation (Figure 5), within each duration the time to minimum pupil diameter (Figure 6A, B, C) and minimum constriction amplitude (Figure 6D, E, F) are similar in the central and peripheral visual fields for the three experimental conditions. The slopes of the regression lines for the pupil constriction data do not differ within each experimental condition (Figure 6D, E, F), and the long wavelength data have smaller PIPR

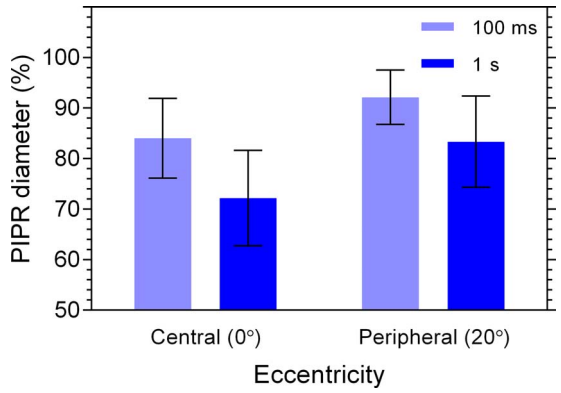

Figure 3. Mean short wavelength PIPR amplitude (±*SD*) for the central and peripheral retina for two stimulus durations. Data are averaged across all conditions (CFD, constant irradiance, and constant field size).

amplitudes than the short wavelength data (Figure 6G, H, I) due to their low melanopsin excitation (Table 1).

Discussion

This study indicates that when pupil diameter is normalized to the pre-stimulus baseline, the post-illumination pupil responses at both retinal eccentricities have a corneal flux density relationship wherein the melanopsin-mediated PIPR amplitude is determined by the product of stimulus irradiance and area. The PIPR amplitude is reduced in the peripheral retina, whereas the minimum pupil constriction does not change in amplitude between the fovea and periphery. Therefore, ipRGC contributions to the PIPR vary with retinal eccentricity but extrinsic inputs to the minimum constriction amplitude do not, indicating that the intrinsic and extrinsic inputs to the pupil control pathway have different eccentricity-dependent spatial summation characteristics.

The hill of vision is a term used in visual perimetry to describe the change in sensitivity across the visual field, where photopic visual sensitivity is highest in the fovea and decreases with increasing eccentricity (Barton & Benatar, 2003; Scott, 1957). Here we observe that in the dark adapted pupil, constriction amplitude did not statistically differ with retinal eccentricity for either the short or long wavelength stimuli (mean reduction in the peripheral retina of 2.9% and 2.5%, respectively), whereas Skorkovská et al. (2014) observed that under light adapted conditions (2.7 cd.m^{-2} background field), the pupil constriction amplitude was ~1 log unit lower at 20° in the peripheral retina compared to the central retina. In contrast to extrinsic inputs to pupil control, the intrinsic pathway mediated short wavelength PIPR amplitude is 0.05 log units (10.3%) more sustained in the central retina than in the temporal retina (Figure 2G, H, I). This decrease in PIPR amplitude is orders of magnitude less than that for photopic light adapted visual thresholds, which are 1 log unit less sensitive in the peripheral retina compared with the central retina (Harvey & Pöppel, 1972; Heijl, Lindgren, & Olsson, 1987; Johnson, Keltner, & Balestrery, 1978).

The pupil constriction amplitude in response to short wavelength stimuli is independent of retinal eccentricity and we infer that the intrinsic ipRGC contributions to this process must be minor. Because constriction amplitude is similar at both eccentricities for both short and long wavelengths, it is likely that extrinsic rod contributions dominate pupil constriction (McDougal & Gamlin, 2010): The short wavelength constriction amplitude increased by 7% in the central retina and

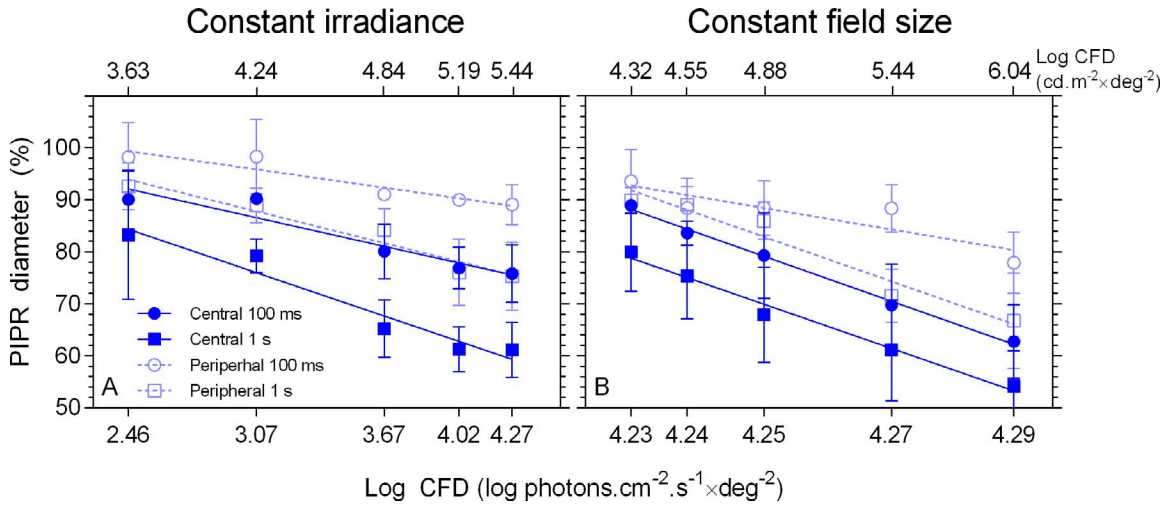

Figure 4. Short wavelength PIPR amplitude for constant irradiance and constant field size conditions plotted as a function of log corneal flux density (±*SD*). Data in panel A and B are transformations of that presented in Figure 2H and 2I, respectively. The log CFD in photometric units (cd.m^{-2} × degrees^{-2}) for the stimuli are indicated on the upper abscissa for each experimental condition.

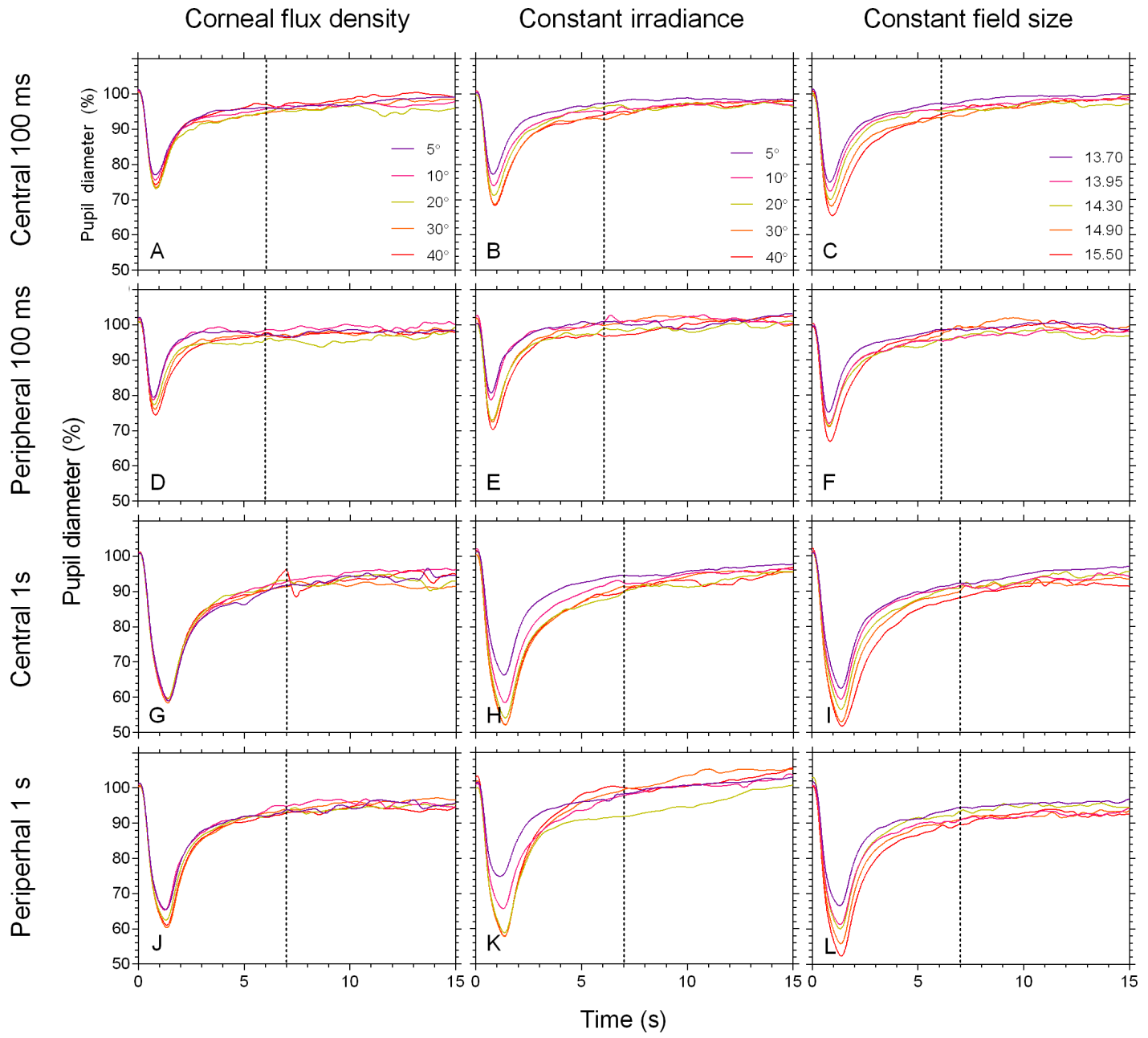

Figure 5. Mean long wavelength pupil tracings for the CFD, constant irradiance, and constant field size conditions ($n = 4$). Normalized (percentage baseline) long wavelength pupil responses are shown as a function of stimulus eccentricity (central 0° and peripheral 20°) and duration (100 ms and 1 s) for 15-s post-stimulus onset (legends are in panels A, B, and C, respectively; panel C legend is in log photons.cm^{-2}.s^{-1}). Dashed vertical lines represent the time the PIPR was quantified.

7.4% in the peripheral retina compared with long wavelength constriction amplitudes, consistent with their high sensitivity to short wavelength light. The response invariance of the constriction amplitude with retinal eccentricity may reflect the rod:cone ratio, which in humans and macaques remains constant at approximately 20 rods per cone between ~10° and ~50° eccentricity from the fovea (Curcio, Sloan, Kalina, & Hendrickson, 1990; Wikler, Williams, & Rakic, 1990), which all stimuli in this study would overlap except the 5° central stimulus. Response invariance across the visual field is not observed with standard perimetry as the photopic light adaptation desensitizes the rods and the cone pathways have higher sensitivity to the test conditions, and thus perceptual thresholds likely reflect the decrease in cone (Curcio et al., 1990; Curcio et al., 1991; Wikler et al., 1990) and ganglion cell density (Curcio & Allen, 1990) with increasing retinal eccentricity (Garway–Heath, Caprioli, Fitzke, & Hitchings, 2000; Harwerth et al., 2002; Harwerth et al., 2004).

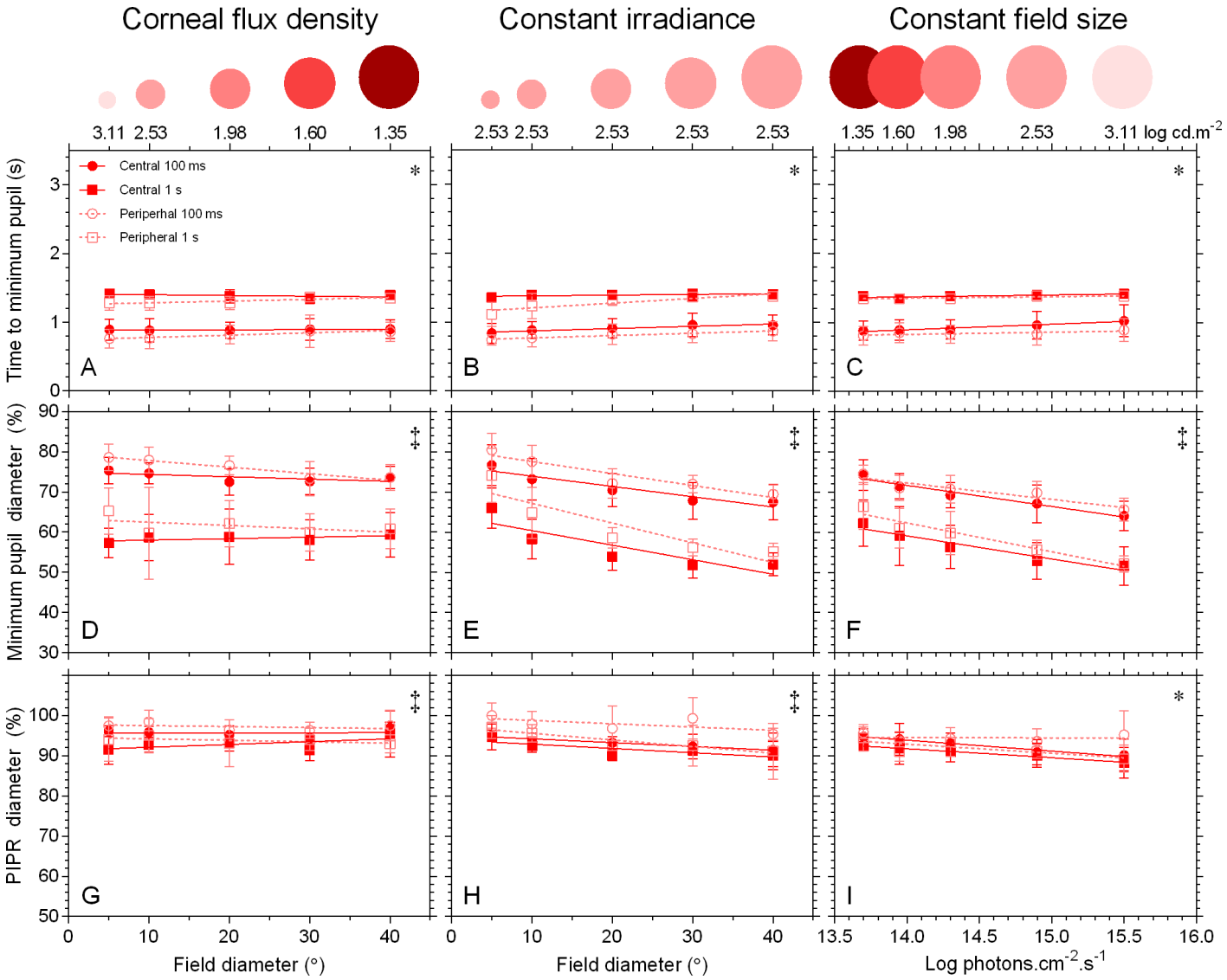

Figure 6. Time to minimum amplitude, minimum amplitude, and PIPR metrics for long wavelength stimuli ($\pm SD$, $n = 4$). Linear regression analysis is shown for the CFD, constant irradiance, and constant field diameter conditions as a function of stimulus eccentricity (central 0° and peripheral 20°) and duration (100 ms and 1 s). * denotes the slopes of all four regression lines are not statistically the same. ‡ denotes the absolute vertical separation of the slopes are statistically different (only determined if slopes are equivalent). A schematic representation of the stimulus diameter and irradiance are shown above the top panels; the log cd.m^{-2} values of the stimuli are indicated on the upper abscissa for the three experimental conditions.

From the observation that the PIPR amplitude to short wavelength light is lower in the peripheral retina than the central retina, we infer that the density of ipRGCs at the two retinal eccentricities and not their dendritic field size primarily governs the PIPR amplitude. Potentially, the higher ipRGC density in the central visual field could increase dendritic overlap, resulting in a higher probabilistic photon catch per unit area than in the peripheral retina where the reduced ipRGC density could lead to lower photon catch by melanopsin. This is supported by physiological data; primate ipRGCs have sparsely branched dendrites but a high degree of overlap (Dacey et al., 2005) including between ipRGCs that stratify in the inner and outer laminae of the inner plexiform layer (Jusuf, Lee, Hannibal, & Grünert, 2007). In humans and macaques however, retinal coverage (the product of dendritic field diameter and density) is uniform with an average of four ipRGC dendrites sampling each point of the visual field (Liao et al., 2016). Given the relatively low expression of melanopsin photopigment per unit area compared with rods and cones (Do et al., 2009), if dendritic field size was the mediating factor then the increased dendritic field size in the periphery would increase the probabilistic photon catch and increase PIPR amplitude rather than the decrease observed in

Figure 2G, H, I. If the lateral plexus formed by ipRGCs determined the PIPR amplitude, then equal amplitudes at both eccentricities would be predicted. Because this was not observed, any functional role of the plexus in generating suprareceptive field (Procyk et al., 2015) contributions to the PIPR must be more localized, rather than operating across the entire visual field.

The reported statistical analyses indicate that linear fits are adequate descriptions of the relationship between PIPR amplitude and field size, although there is evidence in the mean short wavelength data for deviations from the linear model for the non-CFD conditions (Figure 1B, E, F, H, K, L; arrows in Figure 2H and I indicate approximate break point), and these deviations are also present in the individual participant data (see Appendix, Figure A1). It is possible that these deviations from a linear model reflect a critical area for ipRGCs. It is known from psychophysical studies that critical summation areas can be limited by retinal ganglion cell receptive field sizes as exemplified in spatial summation studies of stimuli mediated via the S-cone pathway (inferred koniocellular pathway) where the critical area corresponds to the diameter of the small bistratified ganglion cell receptive fields (Vassilev, Mihaylova, Racheva, Zlatkova, & Anderson, 2003). Sampling the ipRGC receptive fields of transgenic rodless/coneless mice from various locations across the visual field shows that the diameters range between ~15° and ~25° (Procyk et al., 2015). In the constant irradiance 1-s condition, the PIPR amplitudes are larger for fields ≥20° diameter compared with those fields ≤10° (Figure 2H arrow), which is within the range predicted of ipRGC receptive field diameters estimated in the transgenic mouse model (Procyk et al., 2015) and consistent with a report that the PIPR amplitude is minimally sustained for stimuli less than 15° diameter (Park & McAnany, 2013). Maintaining a 40° field (condition 3) indicates that the central visual field PIPR is linear for this condition whereas the peripheral response is not (Figure 2I arrow); that the peripheral PIPR response deviates from the model at the highest irradiance with the 100-ms stimulus, and at the two highest irradiances with the 1-s stimulus, is compatible with the process being driven by the intrinsic melanopsin pathway because melanopsin signalling increases with increasing irradiance and has slower kinetics and longer integration times than rods and cones (Berson, Dunn, & Takao, 2002; Dacey et al., 2005; Gamlin et al., 2007). Reliable estimation of the critical area (if present) from pupil measurements may require factors such as eye movements to be controlled, but the critical area could potentially serve different purposes for image and nonimage-forming functions mediated via ipRGCs.

A primary role of ipRGCs is to integrate photic information (Emanuel & Do, 2015) when signalling external irradiance levels for photoentrainment (Panda et al., 2002) and setting spatial and temporal feature selectivity in visual circuits in mice (Allen et al., 2014), functions that do not require high spatial or temporal resolution. However, melanopsin can also mediate brightness perception in humans (Brown et al., 2012), pattern vision in mice with outer retinal degeneration (Ecker et al., 2010), and modulate the phasic pupil response in humans (Barrionuevo et al., 2014; Joyce et al., 2015), functions that require high spatial and temporal resolution. Here, the decrease in the peripheral PIPR amplitude is not mirrored by a decrease in the peripheral constriction amplitude, which indicates a difference in the spatial tuning characteristics of the extrinsic (rod/cone) and intrinsic (melanopsin) mediated pathways. This is in addition to suggested differences in temporal tuning characteristics (Joyce et al., 2015), evidenced by the increased PIPR amplitudes to the longer duration stimuli at both eccentricities (Figure 2G, H, I). How brain regions (e.g., OPN, SCN, LGN) distinguish between the differing temporal and spatial resolutions of the extrinsic and intrinsic signals encoded by the same ipRGC axon is yet to be determined, and may potentially be accomplished through distinctions in the spike amplitude, frequency, and decays of the ipRGC subtypes (Ecker et al., 2010; Schmidt & Kofuji, 2009; Zhao, Stafford, Godin, King, & Wong, 2014).

For centrally fixated stimuli, the spectral sensitivity of the PIPR measured with stimuli ranging between 7.2° and 41° in diameter closely matches a vitamin A photopigment nomogram at the melanopsin peak sensitivity (~482 nm; Adhikari et al., 2015; Gamlin et al., 2007; Markwell et al., 2010). For the eccentric fixation condition, the decrease in PIPR amplitudes could reflect a shift in the action spectrum of the photopigment mediating the peripheral PIPR. As this is the first study of the peripheral retinal PIPR, its spectral sensitivity has not been characterized. To our knowledge there is no evidence that the spectral sensitivity of melanopsin varies with eccentricity; studies of the spectral sensitivity of in vitro melanopsin ipRGC signalling in macaques (Dacey et al., 2005) and rats (Berson et al., 2002) do not state the retinal eccentricity of their measurements. At present there are no other known photoreceptor that could mediate the sustained signalling after light offset to generate the PIPR, we therefore infer based on the available evidence that melanopsin mediates the peripheral PIPR.

In conclusion, the maximum pupil constriction and post-illumination pupil response components of the human pupil light reflex show different responses in central and peripheral retina; the pupil constriction

amplitude is similar in both the fovea and periphery, unlike the PIPR amplitude which is reduced in the peripheral retina. The pupil control pathway therefore processes extrinsic and intrinsic ipRGC signals differently depending on where in the visual field the signal originates. This observation of the eccentricity dependent reduction in amplitude of melanopsin-mediated pupil response parallels the hill of vision in visual perimetry, whereby sensitivity peaks centrally and reduces with increasing eccentricity. Further finer scale measurement of the PIPR across the visual field will inform the development of pupil perimetry paradigms to assess ocular disease.

Keywords: ipRGC, melanopsin, pupillometry, eccentricity, periphery, corneal flux density

Acknowledgments

This paper was supported by the Australian Research Council Discovery Projects ARC-DP140100333 and an IHBI Vision and Eye Program Grant. We thank Aaron A'brook for technical assistance.

Commercial relationships: none.
Corresponding author: Andrew J. Zele.
Email: andrew.zele@qut.edu.au.
Address: Visual Science Laboratory, Institute of Health and Biomedical Innovation, QUT, Brisbane, Australia.

References

Adhikari, P., Zele, A. J., & Feigl, B. (2015). The post-illumination pupil response (PIPR). *Investigative Ophthalmology and Visual Science*, *56*(6), 3838–3849, doi:10.1167/iovs.14-16233. [PubMed] [Article]

Allen, A. E., Storchi, R., Martial, F. P., Petersen, R. S., Montemurro, M. A., Brown, T. M., & Lucas, R. J. (2014). Melanopsin-driven light adaptation in mouse vision. *Current Biology*, *24*(21), 2481–2490, doi:10.1016/j.cub.2014.09.015.

Alpern, M., McCready, D. W., & Barr, L. (1963). The dependence of the photopupil response on flash duration and intensity. *The Journal of General Physiology*, *47*(2), 265–278, doi:10.1085/jgp.47.2.265.

Atchison, D. A., Girgenti, C. C., Campbell, G. M., Dodds, J. P., Byrnes, T. M., & Zele, A. J. (2011). Influence of field size on pupil diameter under photopic and mesopic light levels. *Clinical and Experimental Optometry*, *94*(6), 545–548, doi:10.1111/j.1444-0938.2011.00636.x.

Barlow, H. B. (1958). Temporal and spatial summation in human vision at different background intensities. *The Journal of Physiology*, *141*(2), 337–350, doi:10.1113/jphysiol.1958.sp005978.

Barrionuevo, P. A., Nicandro, N., McAnany, J. J., Zele, A. J., Gamlin, P., & Cao, D. (2014). Assessing rod, cone and melanopsin contributions to human pupil flicker responses. *Investigative Ophthalmology and Visual Science*, *55*(2), 719–727, doi:10.1167/iovs.13-13252. [PubMed] [Article]

Barton, J. J., & Benatar, M. (2003). *Field of vision: A manual and atlas of perimetry*. New York: Springer Science & Business Media.

Berson, D. M., Dunn, F. A., & Takao, M. (2002). Phototransduction by retinal ganglion cells that set the circadian clock. *Science*, *295*(5557), 1070–1073, doi:10.1126/science.1067262.

Brown, T. M., Tsujimura, S., Allen, A. E., Wynne, J., Bedford, R., Vickery, G., & Lucas, R. J. (2012). Melanopsin-based brightness discrimination in mice and humans. *Current Biology*, *22*, 1–8, doi:10.1016/j.cub.2012.04.039.

Cao, D., Nicandro, N., & Barrionuevo, P. A. (2015). A five-primary photostimulator suitable for studying intrinsically photosensitive retinal ganglion cell functions in humans. *Journal of Vision*, *15*(1), 27, doi:10.1167/15.1.27. [PubMed] [Article]

Crawford, B. H. (1936). The dependence of pupil size upon external light stimulus under static and variable conditions. *Proceedings of the Royal Society of London, Series B, Biological Sciences*, *121*(823), 376–395, doi:10.1098/rspb.1936.0072.

Curcio, C. A., & Allen, K. A. (1990). Topography of ganglion cells in human retina. *Journal of Comparative Neurology*, *300*(1), 5–25, doi:10.1002/cne.903000103.

Curcio, C. A., Allen, K. A., Sloan, K. R., Lerea, C. L., Hurley, J. B., Klock, I. B., & Milam, A. H. (1991). Distribution and morphology of human cone photoreceptors stained with anti-blue opsin. *Journal of Comparative Neurology*, *312*(4), 610–624, doi:10.1002/cne.903120411.

Curcio, C. A., Sloan, K. R., Kalina, R. E., & Hendrickson, A. E. (1990). Human photoreceptor topography. *Journal of Comparative Neurology*, *292*(4), 497–523, doi:10.1002/cne.902920402.

Dacey, D. M., Gamlin, P. D., Liao, H. W., Peterson, B. B., Pokorny, J., Robinson, F. R., & Yau, K. W. (2005). Melanopsin-expressing ganglion cells in primate retina signal colour and irradiance and

project to the LGN. *Nature*, *433*(7027), 749–754, doi:10.1038/nature03387.

Do, M. T. H., Kang, S. H., Xue, T., Zhong, H., Liao, H. W., Bergles, D. E., & Yau, K. W. (2009). Photon capture and signalling by melanopsin retinal ganglion cells. *Nature*, *457*(7227), 281–287, doi:10.1038/nature07682.

Drasdo, N., & Fowler, C. W. (1974). Non-linear projection of the retinal image in a wide-angle schematic eye. *The British Journal of Ophthalmology*, *58*(8), 709–714.

Ecker, J. L., Dumitrescu, O. N., Wong, K. Y., Alam, N. M., Chen, S. K., LeGates, T., & Hattar, S. (2010). Melanopsin-expressing retinal ganglion-cell photoreceptors: cellular diversity and role in pattern vision. *Neuron*, *67*(1), 49–60, doi:10.1016/j.neuron.2010.05.023.

Emanuel, A. J., & Do, M. T. H. (2015). Melanopsin tristability for sustained and broadband phototransduction. *Neuron*, *85*(5), 1043–1055, doi:10.1016/j.neuron.2015.02.011.

Feigl, B., & Zele, A. J. (2014). Melanopsin-expressing intrinsically photosensitive retinal ganglion cells in retinal disease. *Optometry and Vision Science*, *91*(8), 894–903, doi:10.1097/OPX.0000000000000284.

Gamlin, P. D. R., McDougal, D. H., Pokorny, J., Smith, V. C., Yau, K. W., & Dacey, D. M. (2007). Human and macaque pupil responses driven by melanopsin-containing retinal ganglion cells. *Vision Research*, *47*(7), 946–954, doi:10.1016/j.visres.2006.12.015.

Garway–Heath, D. F., Caprioli, J., Fitzke, F. W., & Hitchings, R. A. (2000). Scaling the hill of vision: The physiological relationship between light sensitivity and ganglion cell numbers. *Investigative Ophthalmology and Visual Science*, *41*(7), 1774–1782. [PubMed] [Article]

Hankins, M. W., Peirson, S. N., & Foster, R. G. (2008). Melanopsin: An exciting photopigment. *Trends in Neurosciences*, *31*(1), 27–36, doi:10.1016/j.tins.2007.11.002.

Harvey, L., & Pöppel, E. (1972). Contrast sensitivity of the human retina. *American Journal of Optometry and Archives of American Academy of Optometry*, *49*(9), 748–753, doi:10.1097/00006324-197209000-00007.

Harwerth, R. S., Carter-Dawson, L., Smith, I. I. I. E. L., Barnes, G., Holt, W. F., & Crawford, M. L. J. (2004). Neural losses correlated with visual losses in clinical perimetry. *Investigative Ophthalmology and Visual Science*, *45*(9), 3152–3160, doi:10.1167/iovs.04-0227. [PubMed] [Article]

Harwerth, R. S., Crawford, M. L. J., Frishman, L. J., Viswanathan, S., Smith, E. L., III, & Carter-Dawson, L. (2002). Visual field defects and neural losses from experimental glaucoma. *Progress in Retinal and Eye Research*, *21*(1), 91–125, doi:10.1016/S1350-9462(01)00022-2.

Heijl, A., Lindgren, G., & Olsson, J. (1987). Normal variability of static perimetric threshold values across the central visual field. *Archives of Ophthalmology*, *105*(11), 1544–1549, doi:10.1001/archopht.1987.01060110090039.

Hong, S., Narkiewicz, J., & Kardon, R. H. (2001). Comparison of pupil perimetry and visual perimetry in normal eyes: Decibel sensitivity and variability. *Investigative Ophthalmology and Visual Science*, *42*(5), 957–965. [PubMed] [Article]

Jay, B. S. (1962). The effective pupillary area at varying perimetric angles. *Vision Research*, *1*(5), 418–424, doi:10.1016/0042-6989(62)90021-4.

Johnson, C. A., Keltner, J. L., & Balestrery, F. (1978). Effects of target size and eccentricity on visual detection and resolution. *Vision Research*, *18*(9), 1217–1222, doi:10.1016/0042-6989(78)90106-2.

Joyce, D. S., Feigl, B., Cao, D., & Zele, A. J. (2015). Temporal characteristics of melanopsin inputs to the human pupil light reflex. *Vision Research*, *107*, 58–66, doi:10.1016/j.visres.2014.12.001.

Jusuf, P. R., Lee, S. C. S., Hannibal, J., & Grünert, U. (2007). Characterization and synaptic connectivity of melanopsin-containing ganglion cells in the primate retina. *European Journal of Neuroscience*, *26*(10), 2906–2921, doi:10.1111/j.1460-9568.2007.05924.x.

Kardon, R., Anderson, S. C., Damarjian, T. G., Grace, E. M., Stone, E., & Kawasaki, A. (2009). Chromatic pupil responses. Preferential activation of the melanopsin-mediated versus outer photoreceptor-mediated pupil light reflex. *Ophthalmology*, *116*(8), 1564–1573, doi:10.1016/j.ophtha.2009.02.007.

Kokoschka, S., & Adrian, W. (1985). Influence of field size on the spectral sensitivity of the eye in the photopic and mesopic range. *American Journal of Optometry and Physiological Optics*, *62*(2), 119–126.

Liao, H. W., Ren, X., Peterson, B. B., Marshak, D. W., Yau, K. W., Gamlin, P. D., & Dacey, D. M. (2016). Melanopsin-expressing ganglion cells on macaque and human retinas form two morphologically distinct populations. *Journal of Comparative Neurology*, in press, doi:10.1002/cne.23995.

Lucas, R. J., Peirson, S. N., Berson, D. M., Brown, T. M., Cooper, H. M., Czeisler, C. A., & Brainard, G. C. (2014). Measuring and using light in the

melanopsin age. *Trends in Neurosciences*, *37*(1), 1–9, doi:10.1016/j.tins.2013.10.004.

Markwell, E. L., Feigl, B., & Zele, A. J. (2010). Intrinsically photosensitive melanopsin retinal ganglion cell contributions to the pupillary light reflex and circadian rhythm. *Clinical and Experimental Optometry*, *93*(3), 137–149, doi:10.1111/j.1444-0938.2010.00479.x.

Mathur, A., Gehrmann, J., & Atchison, D. A. (2013). Pupil shape as viewed along the horizontal visual field. *Journal of Vision*, *13*(6):3, 1–8, doi:10.1167/13.6.3. [PubMed] [Article]

McDougal, D. H., & Gamlin, P. D. (2010). The influence of intrinsically-photosensitive retinal ganglion cells on the spectral sensitivity and response dynamics of the human pupillary light reflex. *Vision Research*, *50*(1), 72–87, doi:10.1016/j.visres.2009.10.012.

McDougal, D. H., & Gamlin, P. D. (2015). Autonomic control of the eye. *Comprehensive Physiology*, *5*(1), 439–473, doi:10.1002/cphy.c140014.

Mure, L. S., Cornut, P. L., Rieux, C., Drouyer, E., Denis, P., Gronfier, C., & Cooper, H. M. (2009). Melanopsin bistability: A fly's eye technology in the human retina. *PLoS One*, *4*(6), e5991, doi:10.1371/journal.pone.0005991.

Mure, L. S., Rieux, C., Hattar, S., & Cooper, H. M. (2007). Melanopsin-dependent nonvisual responses: evidence for photopigment bistability in vivo. *Journal of Biological Rhythms*, *22*(5), 411–424, doi:10.1177/0748730407306043.

Panda, S., Sato, T. K., Castrucci, A. M., Rollag, M. D., DeGrip, W. J., Hogenesch, J. B., & Kay, S. A. (2002). Melanopsin (Opn4) requirement for normal light-induced circadian phase shifting. *Science*, *298*(5601), 2213–2216, doi:10.1126/science.1076848.

Park, J. C., & McAnany, J. J. (2013). Spatial summation characteristics of the pupillary light reflex differ under rod-, cone- and melanopsin-mediated conditions. *Journal of Vision*, *13*(15): 38, doi:10.1167/13.15.38. [Abstract]

Park, J. C., & McAnany, J. J. (2015). Effect of stimulus size and luminance on the rod-, cone-, and melanopsin-mediated pupillary light reflex. *Journal of Vision*, *15*(3):13, 1–13, doi:10.1167/15.3.13. [PubMed] [Article]

Park, J. C., Moura, A. L., Raza, A. S., Rhee, D. W., Kardon, R. H., & Hood, D. C. (2011). Toward a clinical protocol for assessing rod, cone, and melanopsin contributions to the human pupil response. *Investigative Ophthalmology and Visual Science*, *52*(9), 6624–6635. [PubMed] [Article]

Pokorny, J., & Smith, V. (1997). How much light reaches the retina? *Documenta Ophthalmologica Proceedings Series*, *59*, 491–512, doi:10.1007/978-94-011-5408-6_56.

Procyk, C. A., Eleftheriou, C. G., Storchi, R., Allen, A. E., Milosavljevic, N., Brown, T. M., & Lucas, R. J. (2015). Spatial receptive fields in the retina and dorsal lateral geniculate nucleus (dLGN) of mice lacking rods and cones. *Journal of Neurophysiology*, *114*(2), 1321–1330, doi:10.1152/jn.00368.2015.

Provencio, I., Rollag, M. D., & Castrucci, A. M. (2002). Photoreceptive net in the mammalian retina. *Nature*, *415*(6871), 493–493, doi:10.1038/415493a.

Schmidt, T. M., & Kofuji, P. (2009). Functional and morphological differences among intrinsically photosensitive retinal ganglion cells. *The Journal of Neuroscience*, *29*(2), 476–482, doi:10.1523/JNEUROSCI.4117-08.2009.

Schweitzer, N. M. J. (1956). Threshold measurements on the light reflex of the pupil in the dark adapted eye. *Documenta Ophthalmologica*, *10*(1), 1–78, doi:10.1007/BF00172098.

Scott, G. I. (1957). *Traquair's Clinical Perimetry (7th ed.)*. London: Henry Kimpton.

Sekaran, S., Foster, R. G., Lucas, R. J., & Hankins, M. W. (2003). Calcium imaging reveals a network of intrinsically light-sensitive inner-retinal neurons. *Current Biology*, *13*(15), 1290–1298, doi:10.1016/S0960-9822(03)00510-4.

Skorkovská, K., Wilhelm, H., Lüdtke, H., Wilhelm, B., & Kurtenbach, A. (2014). Investigation of summation mechanisms in the pupillomotor system. *Graefe's Archive for Clinical and Experimental Ophthalmology*, *252*(7), 1155–1160, doi:10.1007/s00417-014-2677-4.

Spitschan, M., Jain, S., Brainard, D. H., & Aguirre, G. K. (2014). Opponent melanopsin and S-cone signals in the human pupillary light response. *Proceedings of the National Academy of Sciences, USA. 111*(43), 15568–15572, doi:10.1073/pnas.1400942111.

Spring, K. H., & Stiles, W. S. (1948). Variation of pupil size with change in the angle at which the light stimulus strikes the retina. *The British Journal of Ophthalmology*, *32*(6), 340–346, doi:10.1136/bjo.32.6.340.

Stabell, U., & Stabell, B. (1980). Variation in density of macular pigmentation and in short-wave cone sensitivity with eccentricity. *Journal of the Optical Society of America*, *70*(6), 706–711, doi:10.1364/JOSA.70.000706.

Stanley, P. A., & Davies, A. K. (1995). The effect of field of view size on steady-state pupil diameter.

Ophthalmic and Physiological Optics, *15*(6), 601–603, doi:10.1046/j.1475-1313.1995.9400019v.x.

Tsujimura, S., Ukai, K., Ohama, D., Nuruki, A., & Yunokuchi, K. (2010). Contribution of human melanopsin retinal ganglion cells to steady-state pupil responses. *Proceedings of the Royal Society B: Biological Sciences*, *277*(1693), 2485–2492, doi:10.1098/rspb.2010.0330.

van de Kraats, J., & van Norren, D. (2007). Optical density of the aging human ocular media in the visible and the UV. *Journal of the Optical Society of America, A*, *24*(7), 1842–1857, doi:10.1364/JOSAA.24.001842.

van Esch, J. A., Koldenhof, E. E., van Doorn, A. J., & Koenderink, J. J. (1984). Spectral sensitivity and wavelength discrimination of the human peripheral visual field. *Journal of the Optical Society of America A*, *1*(5), 443–450, doi:10.1364/JOSAA.1.000443.

Vassilev, A., Mihaylova, M. S., Racheva, K., Zlatkova, M., & Anderson, R. S. (2003). Spatial summation of S-cone ON and OFF signals: Effects of retinal eccentricity. *Vision Research*, *43*(27), 2875–2884, doi:10.1016/j.visres.2003.08.002.

Vervoort, H. (1899). Die Reaction der pupille bei der accommodation und der convergenz und bei der beleuchtung verschieden grosser flächen der retina mit einer constanten lichtmenge. *Albrecht von Graefes Archiv für Ophthalmologie*, *49*(2), 348–374, doi:10.1007/bf02012684.

Viénot, F., Bailacq, S., & Rohellec, J. L. (2010). The effect of controlled photopigment excitations on pupil aperture. *Ophthalmic and Physiological Optics*, *30*(5), 484–491, doi:10.1111/j.1475-1313.2010.00754.x.

Watson, A. B., & Yellott, J. I. (2012). A unified formula for light-adapted pupil size. *Journal of Vision*, *12*(10):12, 1–16, doi:10.1167/12.10.12. [PubMed] [Article]

Webster, J. G. (1969). Critical duration for the pupillary light reflex. *Journal of the Optical Society of America*, *59*(11), 1473–1478, doi:10.1364/JOSA.59.001473.

Wikler, K. C., Williams, R. W., & Rakic, P. (1990). Photoreceptor mosaic: Number and distribution of rods and cones in the rhesus monkey retina. *Journal of Comparative Neurology*, *297*(4), 499–508, doi:10.1002/cne.902970404.

Wilson, M. (1970). Invariant features of spatial summation with changing locus in the visual field. *The Journal of Physiology*, *207*(3), 611–622, doi:10.1113/jphysiol.1970.sp009083.

Wooten, B. R., Hammond, B. R., Land, R. I., & Snodderly, D. M. (1999). A practical method for measuring macular pigment optical density. *Investigative Ophthalmology and Visual Science*, *40*(11), 2481–2489. [PubMed] [Article]

Xu, J., Pokorny, J., & Smith, V. C. (1997). Optical density of the human lens. *Journal of the Optical Society of America, A*, *14*(5), 953–960, doi:10.1364/JOSAA.14.000953.

Zele, A. J., Feigl, B., Smith, S. S., & Markwell, E. L. (2011). The circadian response of intrinsically photosensitive retinal ganglion cells. *PLoS One*, *6*(3), e17860, doi:10.1371/journal.pone.0017860.

Zhao, X., Stafford, B. K., Godin, A. L., King, W. M., & Wong, K. Y. (2014). Photoresponse diversity among the five types of intrinsically photosensitive retinal ganglion cells. *The Journal of Physiology*, *592*(7), 1619–1636, doi:10.1113/jphysiol.2013.262782.

Appendix

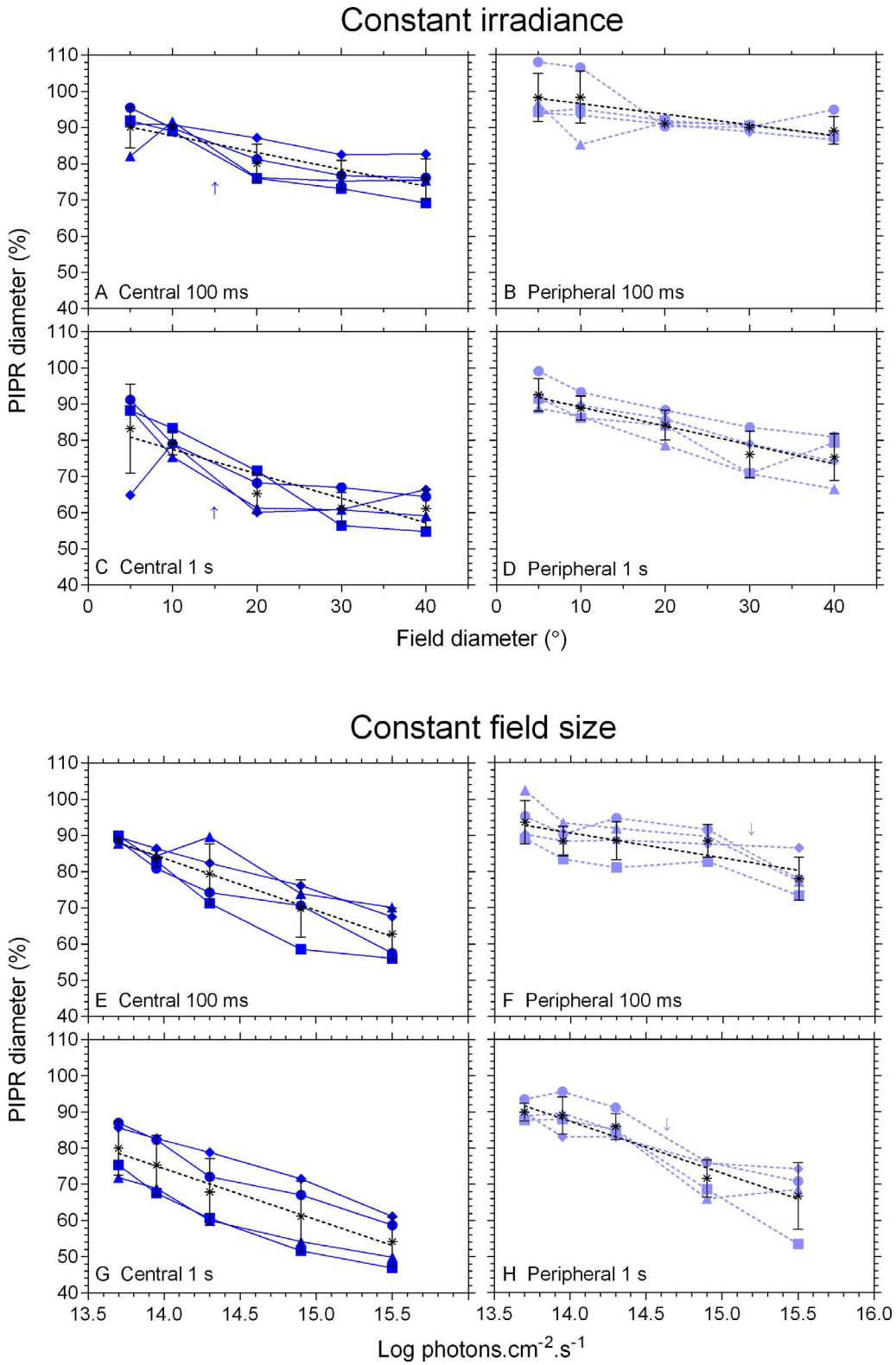

Figure A1. Individual data sets for four observers comprising Figure 2H (Panels A, B, C, D) and Figure 2I (Panels E, F, G, H). Each data point (blue symbol) is the average of four repeats (±*SD*). Black symbols indicate mean data and trend line. Arrows in panels A, C, F, and H denote the trends observed in Figure 2 and Discussion.